Electronic structure of deep-lying sulfur centers in Si

W. E. Krag,* W. H. Kleiner,† and H. J. Zeiger
Lincoln Laboratory, Massachusetts Institute of Technology, Lexington, Massachusetts 02173-0073
(Received 29 January 1986)

A theoretical analysis has been made of infrared absorption spectra measured earlier for four deep-lying sulfur donor centers in Si. The analysis is based on a group-theoretic treatment for the behavior of electronic levels under uniaxial stress. The data consist of absorption frequencies and polarization selection rules determined for calibrated uniaxial stress applied along the [001], [111], and [110] axes. Both $1s \rightarrow np$ transitions and $1s \rightarrow 1s$ transitions are observed. The A and B centers (binding energies 0.1095 and 0.1877 eV, respectively) are found to be He-like, while the C and D centers (binding energies 0.3705 and 0.6136 eV, respectively) are found to be He^+-like. The D-center spectra are consistent with T_d symmetry, while the A-, B-, and C-center spectra are consistent in most respects with C_{3v} or D_{3d} symmetry. The analysis of the $1s \rightarrow np$ spectra yields values of ~ 7.9 eV for the conduction-band pure shear deformation potential, somewhat lower than the value of ~ 10 eV determined from spin-resonance experiments. A well-defined $1s(A_1)_{\text{ground}} \rightarrow 1s(T_2)$ spectrum is observed for the D center; $1s(A_1)_{\text{ground}} \rightarrow 1s(E)$ and $1s(A_1)_{\text{ground}} \rightarrow 1s(A_1)$ spectra are observed for the B center. From comparison of the data with theory, parameters of the ground and excited levels are determined. One noteworthy result is the finding that the $1s \rightarrow np$ spectral frequencies observed under stress for the A center are consistent with a twofold-degenerate $1s(E)$ ground state.

I. INTRODUCTION

The study of impurity states in semiconductors was given great impetus by the early experiments of Burstein *et al.*[1] on the infrared-absorption spectra of shallow donors in Si and Ge, together with the theoretical analysis of these spectra by Kohn and Luttinger.[2] More recently, the properties of deep-lying impurity states in semiconductors have attracted great interest because such states can have an important influence on the performance of semiconductor devices. In this paper we report a study of the electronic structure of four deep-lying S centers in Si. This study involves a detailed analysis of earlier data[3] on the infrared-absorption spectra of S-doped Si measured at ~ 10 K as a function of calibrated uniaxial stress.

There have been a number of recent, detailed studies of the infrared-absorption spectra of S and other chalcogenides in Si in the absence of stress.[4] The study of such spectra in the presence of calibrated uniaxial stress adds considerably to the power of the experiments, yielding information on the stress-dependent Hamiltonians and symmetries of the states observed, as well as information on the impurity site symmetries. A recent study[5] of this type on oxygen-associated states in Si has helped greatly in elucidating the nature of these states.

The first theoretical treatment of donor states in Si (Ref. 2) applied to shallow donors. This treatment was based on the effective-mass approximation (EMA), according to which the states are derived from linear combinations of contributions from the six conduction-band minima in a manner appropriate to the state symmetries. The theory assumed further that the behavior of states under applied stress is given by the deformation-potential approximation (DPA),[6] which describes the changes in energy of the conduction-band edges with stress. More recent theoretical treatment of the deeper-lying chalcogenide donor states[7] indicates that these states deviate considerably from an EMA description.

The four S centers discussed in this paper, which we designate as A, B, C, and D,[8] have ground states lying, respectively, 0.1095, 0.1877, 0.3705, and 0.6136 eV below the conduction-band edge.[3] Their excited np_0 and $np_\pm$ levels are well described by the EMA and DPA. Their ground states and low-lying excited states are derived from $1s$-like states, but are considerably perturbed from the simple EMA description, as expected for moderately deep-lying levels. However, the framework of the EMA is adequate for obtaining the symmetries of these levels. Using these symmetries, we have employed group-theoretic arguments to derive expressions giving the energies of the levels as functions of the magnitude and orientation of applied stress. These expressions have been compared with experimental results to obtain parameter values describing the stress behavior of the levels. The measured values are found to deviate considerably from those predicted by EMA-DPA theory.

In Sec. II of this paper we describe briefly the sample preparation and experimental apparatus used in our study of the S centers in Si. The theoretical description of energy-level behavior under uniaxial stress is given in Sec. III. In Sec. IV the analysis of the spectra of the four centers is presented. The centers are discussed in the order of our decreasing understanding of their electronic structure.

II. EXPERIMENTAL DETAILS

A. Sample preparation

Samples to be doped with S were cut from Si boules to a size of $13 \times 13 \times 4$ mm^3, with the cut faces oriented by x-ray diffraction. The boules were either nominally un-

doped (with resistivities up to several thousand ohm-centimeters) or doped with B to 10^{16} cm^{-3}, depending on whether the S centers were to be neutral or ionized. The samples were ground, cleaned in hydrogen fluoride etch, and rinsed with water and alcohol. Each sample was then placed in a fused silica ampoule with approximately 3 mg of 99.99%-pure sulfur. The ampoule was sealed off under vacuum, placed in a furnace, and maintained at a temperature of 1280 °C for about 30 h. After this period, either the ampoule was pushed out of the furnace into a bath of ethylene glycol for rapid cooling, or the furnace was turned off and the sample allowed to cool in place. After cooling, the sample was removed from the ampoule, the faces were ground, and the electrical type and resistivity were checked. All the measured samples were n type. The sample was then polished to a size of $10\times10\times2.5$ mm^3, with the opposite faces plane and parallel to 1 μm.

B. Measuring apparatus

The sample was placed on the base plate of a vacuum chamber that was in thermal contact with the copper bottom of a Dewar containing liquid helium (see Fig. 1). Stress was applied by means of a stainless-steel rod that was enclosed in a stainless-steel tube and passed through the Dewar to an anvil on top of the sample. The force was provided by nitrogen gas from a cylinder connected to a calibrated air piston that was attached to the top of the Dewar. To obtain uniform stress on the upper and lower faces of the sample, Teflon spacers were inserted between these faces and the anvil and base plate, which had machined surfaces. The maximum total force applied was usually about 400 lb, though some spectra were measured to values about 20% higher. The monochromator was a Perkin-Elmer model 98 modified for use with a foreprism, and a Princeton Applied Research lock-in amplifier was used as the main amplifier. The Dewar was placed in the afteroptics of the monochromator, with the sample oriented so that the monochromatic beam passed through a 1-cm length of silicon. The highest absorption coefficient measured for any of the transitions was about 4 cm^{-1}.

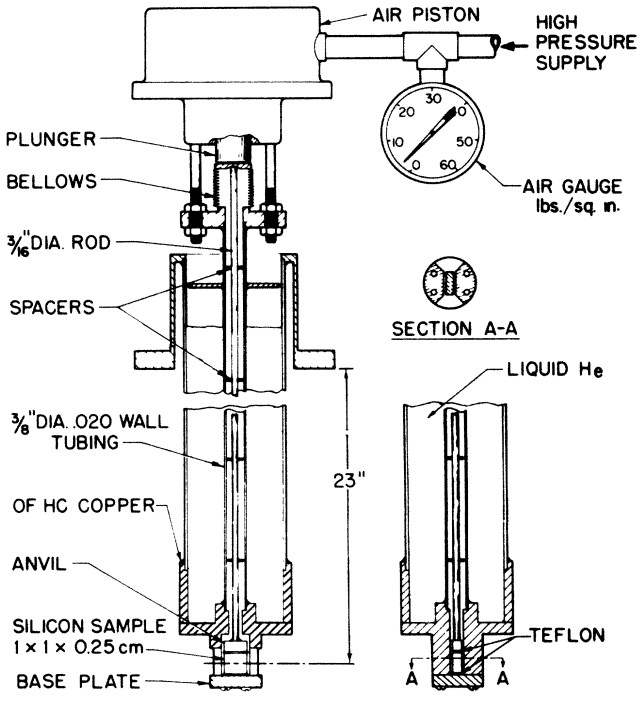

FIG. 1. Sketch of apparatus for measuring infrared-absorption spectra under calibrated uniaxial stress.

III. THEORETICAL DESCRIPTION OF SPECTRA IN THE PRESENCE OF STRESS

A. $1s\rightarrow np$ spectra in the EMA and DPA

The conduction band of Si consists of six band-edge minima located along [100] axes in **k** space, at approximately 0.85 of the distance to the X point. The constant-energy surfaces associated with the band edges are somewhat cigar-shaped, with effective masses $m_t/m_0=0.192$ and $m_l/m_0=0.90$. These masses have been used by Kohn[2] and later by Faulkner[9] to predict the energy levels of hydrogenic donors in the EMA. The levels calculated by Faulkner are shown in Fig. 2, along with the positions of the levels deduced from experiment for the A, B, C, and D centers of S in Si.[3] (The data are summarized in Tables I and II. Some of the identifications of weak transitions come from Ref. 10.) In plotting the positions of the experimental levels, we have aligned the $2p_\pm$ levels from experiment with the calculated $2p_\pm$ levels. The A and B centers have been identified[3] as neutral S centers, which are analogs of the He atom. Since the excited states of He form a hydrogen-atom-like series, we can expect the plot of the A and B excited p states to match reasonably the calculated effective-mass spectrum of a hydrogenic donor with $Z=1$, as it indeed does. On the other hand, the C and D centers have been identified[3] as singly charged He^+-like centers with $Z=2$, which suggests that the energies of the excited levels relative to the band edge are a factor of 4 larger than they would be for a hydrogen-like center. Accordingly, the experimental spacings between levels for the C and D spectra in Fig. 2 have been scaled down by a factor of 4 for comparison with the hydrogenic effective-mass levels. A more detailed comparison of the experimental spectra with the calculated effective-mass spectra is deferred to Sec. IV.

The $1s$-like levels for donors in Si in the EMA are written as

$$\Psi(\mathbf{r})=\sum_{j=1}^{6}\alpha_j F_j(\mathbf{r})\phi_j(\mathbf{r})\ , \tag{1}$$

where the α_j are coefficients, and $F_j(\mathbf{r})$ and $\phi_j(\mathbf{r})$ are, respectively, envelope functions and Bloch functions at each conduction-band edge. The $1s$ envelope functions have nonvanishing wave functions at the origin, and are therefore subject to a central-cell perturbation at the position of the donor atom.[2] This perturbation mixes wave functions from the six electron minima and lifts their degeneracy, producing states (in the usual substitutional T_d symmetry)

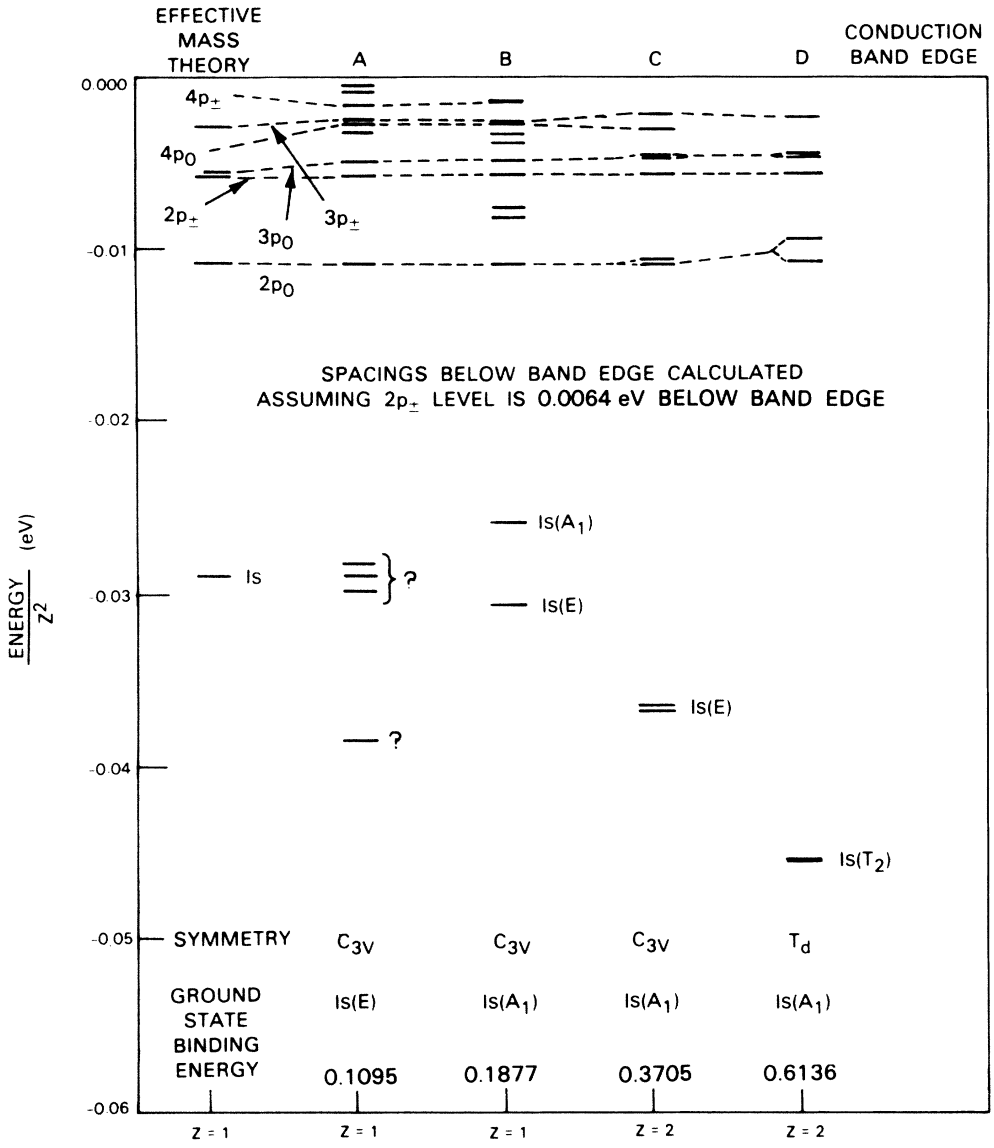

FIG. 2. Energy-level diagram for S centers determined by infrared-absorption measurements.

$$\psi_{1s}(A_1)=(1/\sqrt{6})(1,1,1,1,1,1)\ \ (1)\ , \tag{1a}$$

$$\psi_{1s}(E)=\begin{cases}(1/\sqrt{12})(-1,-1,-1,-1,2,2) \\ \qquad\qquad (2z^2-x^2-y^2)\ , \\ \frac{1}{2}(1,1,-1,-1,0,0)\ \ [\sqrt{3}(x^2-y^2)]\ ,\end{cases} \tag{1b}$$

$$\psi_{1s}(T_2)=\begin{cases}(1/\sqrt{2})(1,-1,0,0,0,0)\ \ (x)\ , \\ (1/\sqrt{2})(0,0,1,-1,0,0)\ \ (y)\ , \\ (1/\sqrt{2})(0,0,0,0,1,-1)\ \ (z)\ .\end{cases} \tag{1c}$$

The ordered entries give the coefficients α_j of the contribution to the wave function from the valleys along the axes $(\hat{\mathbf{x}},-\hat{\mathbf{x}},\hat{\mathbf{y}},-\hat{\mathbf{y}},\hat{\mathbf{z}},-\hat{\mathbf{z}})$. The terms to the right give the transformation properties of the wave functions. For most simple hydrogenic donors, the $1s(A_1)$ state is the ground state, while the $1s(E)$ and $1s(T_2)$ states are closer in energy to the effective-mass $1s$ state.

The *np*-like levels, which have vanishing wave functions at the origin in EMA, are only weakly affected by the central-cell perturbation, and therefore usually retain their sixfold valley degeneracy. For the *C* center, which has non-T_d symmetry, the *np* levels show small splittings (see Sec. IV C).

In the presence of strain, the *j*th valley in Si shifts by an amount

$$\Delta\mathscr{E}^{(j)}=E_1\underline{I}:\underline{\epsilon}+E_2(\hat{\mathbf{j}}\hat{\mathbf{j}}-\tfrac{1}{3}\underline{I}):\underline{\epsilon}\ , \tag{2}$$

where E_1 is the dilatational deformation potential, E_2 is the pure shear deformation potential, $\underline{\epsilon}$ is the strain tensor, and $\underline{I}$ is the 3×3 identity matrix. The strain due to an applied stress $\underline{T}$ is

$$\underline{\epsilon}=\underline{S}\cdot\underline{T}\ ,$$

where $\underline{S}$ is the elastic compliance tensor. If the applied

TABLE I. Transition energies for sulfur centers in silicon.

Transition	Transition energy (eV) A	B	C	D
$1s \rightarrow 1s$	0.070 45		0.220 96	
	0.079 03		0.221 61	
	0.079 98	0.156 41	0.221 94	0.429 34
	0.8070	0.161 20	0.225 76	0.429 68
$1s \rightarrow 2p_0$	0.097 91	0.176 15	0.323 60 0.324 79	0.567 97 0.573 01
$1s \rightarrow 2p_\pm$	0.103 13	0.181 26	0.344 53 0.344 89	0.587 95
$1s \rightarrow 3p_0$	0.104 03	0.182 15	0.348 44 0.348 99	0.592 08 0.593 03
$1s \rightarrow 3p_\pm$	0.106 42	0.184 52	0.358 68	0.601 38
$1s \rightarrow 4p_0$	0.106 19	0.184 34		
$1s \rightarrow 4p_\pm$	0.107 34	0.185 49		
$1s \rightarrow 5p_\pm$		0.186 21		
Weak				
$1s \rightarrow 3d_0$	0.105 70	0.183 76	0.355 51	0.598 52
$1s \rightarrow 2s(E)$ (A_1)		0.178 82 0.179 45	0.340 06	0.573 04
$1s \rightarrow 3s(E)$ (A_1)		0.182 86 0.183 10		0.593 08
	0.108 11 0.108 49	0.185 70		

TABLE II. Calculated and observed energy levels for sulfur centers in silicon.

Level	Calculated EM (eV)	Observed A (eV)	B (eV)	C/4 (eV)	D/4 (eV)
Ground state	−0.031 27	−0.1095	−0.1877	−0.3705/4	−0.6136/4
$2p_0$	−0.011 51	−0.011 59	−0.011 55	−0.011 73 −0.011 43	−0.011 408 −0.010 15
$2p_\pm$	−0.006 40	−0.006 37	−0.006 44	−0.006 49 −0.006 40	−0.006 41
$3p_0$	−0.005 48	−0.005 47	−0.005 55	−0.005 52 −0.005 38	−0.005 38 −0.005 14
$3p_\pm$	−0.003 12	−0.003 08	−0.003 18	−0.002 96	−0.003 06
$4p_0$	−0.003 33	−0.003 31	−0.003 36		
$4p_\pm$	−0.002 19	−0.002 16	−0.002 21		
$5p_\pm$	−0.001 44		−0.001 49		
$2s(E)$ (A_1)	−0.008 83		−0.008 88 −0.008 25	−0.007 61	−0.010 14
$3s(E)$ (A_1)	−0.004 75		−0.004 84 −0.004 60		−0.005 13
$3d_0$	−0.003 75	−0.003 80	−0.003 94	−0.003 75	−0.003 77

stress is purely compressional along the direction $\hat{\mathbf{n}}$, then $\underline{T}=T\hat{\mathbf{n}}\hat{\mathbf{n}}$. (Note that T is *negative* for compression.) In that case, for the jth valley,[6]

$$\Delta\mathscr{E}^{(j)}=E_1(S_{11}+2S_{12})T+E_2(S_{11}-S_{12})(n_j^2-\tfrac{1}{3})T\ , \tag{3}$$

where n_j is the component of the vector $\hat{\mathbf{n}}$ along the jth valley axis.

Since the np levels for the six valleys are essentially degenerate in the EMA, Eq. (3) describes how these levels will shift and split in the DPA with the application of a compressional stress along the $\hat{\mathbf{n}}$ direction. Combining Eq. (3) with Eq. (1a), we also see that the $1s(A_1)$ ground state in T_d symmetry should shift under stress by

$$\Delta\mathscr{E}_{1s}(A_1)=E_1'(S_{11}+2S_{12})T\ , \tag{4}$$

where E_1' may not be quite the same as E_1, since the ground state may contain an additional small contribution outside the EMA from other bands. If E_1 and E_1' are the same, then the center of gravity of the $1s(A_1)\rightarrow np$ spectrum should not shift under applied stress. As noted above, for deep donors the EMA may not be accurate, and the DPA description of the effect of strain may not be adequate (see Sec. III B).

The np_0 and $np_\pm$ levels are eigenstates of angular-momentum component L_z, although they are not eigenstates of total angular momentum $\mathbf{L}^2$. The $np_\pm$ levels are degenerate, but they are not degenerate with np_0 (see Fig. 2). The relative intensities of $1s(A_1)\rightarrow np_\pm$ and $1s(A_1)\rightarrow np_0$ electric-dipole transitions associated with the jth valley are, respectively,

$$\begin{aligned} I^j_{np_\pm}&=(\hat{\mathbf{E}}\times\hat{\mathbf{j}})^2\,|\,M_{np_\pm}\,|^2\ ,\\ I^j_{np_0}&=(\hat{\mathbf{E}}\cdot\hat{\mathbf{j}})^2\,|\,M_{np_0}\,|^2 \end{aligned} \tag{5}$$

where $\hat{\mathbf{E}}$ is a unit vector along the optical electric field and $\hat{\mathbf{j}}$ is a unit vector along the jth-valley axis [see Appendix, Eq. (A12)].

We make use of Eqs. (3) and (5) to analyze the $1s\rightarrow np$ spectra observed for the four S centers studied. There is clear evidence from the stress dependence of these spectra that three of the centers are not located in sites of T_d symmetry. The A, B, and C centers all appear to occupy sites with trigonal symmetry (either C_{3v} or D_{3d}), the symmetry axes for the centers being distributed randomly along $\langle 111\rangle$ directions. For either C_{3v} or D_{3d} symmetry, a site has a threefold symmetry axis and three reflection planes containing the symmetry axis and making 120° angles with respect to one another. In addition, a site of D_{3d} symmetry has a center of inversion. For our purposes, then, the main difference between C_{3v} and D_{3d} symmetry is that in D_{3d} symmetry eigenstates are of either odd or even parity, while in C_{3v} symmetry they are of mixed parity. This difference can affect the stress dependence of energy levels and selection rules, allowing us, in principle, to distinguish between the two cases. In fact, we have not been able to distinguish convincingly between the two cases from any of our experimental results.

It should be noted, however, that C_{3v} and D_{3d} symmetry imply very different geometries for defect centers in Si. A center which is formed by a slight distortion from a site of T_d symmetry cannot have inversion symmetry, and therefore cannot have D_{3d} symmetry. A center which has D_{3d} symmetry is almost certainly located at a site which has D_{3d} symmetry in the perfect Si lattice.

A perturbation of C_{3v} or D_{3d} symmetry causes a T_2 state in T_d symmetry to break up into $E+A_1$ states, producing $1s$-like states in the EMA of the form

$$\psi_{1s(A_1)}=(1/\sqrt{6})(1,1,1,1,1,1)\ \ (1)\ , \tag{6a}$$

$$\psi_{1s(E)}=\begin{cases}(1/\sqrt{12})(-1,-1,-1,-1,2,2)\\ \qquad\qquad (2z^2-x^2-y^2)\ ,\\ \frac{1}{2}(1,1-1,-1,0,0)\ \ [\sqrt{3}(x^2-y^2)]\ ,\end{cases} \tag{6b}$$

$$\psi_{1s(E')}=\begin{cases}(1/\sqrt{12})(-1,1,-1,1,2,-2)\ \ (2z-x-y)\ ,\\ \frac{1}{2}(1,-1,-1,1,0,0)\ \ [\sqrt{3}(x-y)]\ ,\end{cases} \tag{6c}$$

$$\psi_{1s(A_1')}=(1/\sqrt{6})(1,-1,1,-1,1,-1)\ \ (x+y+z)\ . \tag{6d}$$

For a C_{3v} perturbation, the A_1 and A_1' states and the E and E' states will also be admixed, giving states of mixed parity.

B. Spectra of donors outside the EMA-DPA: T_d symmetry

Although the EMA combined with the DPA seems to work well in describing $1s$ and np states of shallow donors such as P, As, and Sb in Si (binding energies $\sim$0.04—0.05 eV), it is not adequate to give an accurate description of the behavior of S in Si (binding energies $\sim$0.1—0.6 eV). It has been shown from spin-resonance hyperfine-splitting data[11] that the D-center ground-state wave function differs strongly from that predicted by the EMA theory, although the D center appears to occupy a site of T_d symmetry.

The general Hamiltonian describing the behavior of a set of levels in the presence of strain can be written as

$$H_{\rm str}=\sum_{\alpha,\beta}U_{\alpha\beta}\epsilon_{\alpha\beta}\ , \tag{7}$$

where the coefficients $U_{\alpha\beta}$ are symmetric functions of donor-electron coordinates ($U_{\alpha\beta}=U_{\beta\alpha}$). For a given center, the $U_{\alpha\beta}$'s describing one set of donor levels may not be the same as those describing another set, since the admixture of contributions from different band edges may not be the same for different states.

In the case of T_d symmetry, it is useful to rewrite Eq. (7) in the form where the combinations of U's appearing transform explicitly as bases of irreducible representations of the T_d group. The result is

$$H_{\rm str}=a_1\Delta+\tfrac{1}{6}G_1\epsilon_1+\tfrac{1}{6}G_2\epsilon_2+\sum_\alpha V_\alpha\tau_\alpha\ , \tag{8}$$

where

$$\begin{aligned} &\Delta\equiv\sum_\alpha\epsilon_{\alpha\alpha},\ \ A_1\ ,\\ &\left.\begin{aligned}\epsilon_1&\equiv 2\epsilon_{zz}-\epsilon_{xx}-\epsilon_{yy},\\ \epsilon_2&\equiv\sqrt{3}(\epsilon_{xx}-\epsilon_{yy}),\end{aligned}\right\}\ E\ ,\\ &\tau_x=\epsilon_{yz},\ \ \tau_y=\epsilon_{zx},\ \ \tau_z=\epsilon_{xy},\ \ T_2\ , \end{aligned} \tag{8a}$$

$$a_1 \equiv \tfrac{1}{3}\sum_{\alpha} U_{\alpha\alpha},\quad A_1$$
$$\left.\begin{aligned} G_1 &\equiv 2U_{zz}-U_{xx}-U_{yy},\\ G_2 &\equiv \sqrt{3}(U_{xx}-U_{yy}),\end{aligned}\right\} E\ , \tag{8b}$$
$$V_x = U_{yz},\quad V_y = U_{zx},\quad V_z = U_{xy},\quad T_2\ .$$

In these equations, the subscripts x,y,z refer to cubic axes in the crystal.

The strain energy of the $1s(A_1)$ level can be calculated from Eq. (8) by noting that the only term having a nonvanishing matrix element with respect to an A_1 state is the term with spatial dependence transforming as A_1. The result for the energy, writing the strain in terms of stress and elastic compliance coefficients, is of the form

$$\mathscr{E}(A_1) = \mathscr{E}_0(A_1) + a(S_{11}+2S_{12})T\ , \tag{9}$$

where $a = \langle A_1 \mid \frac{1}{3}\sum_{\alpha} U_{\alpha\alpha} \mid A_1 \rangle$. This is the same result we would get from the EMA wave function, given by Eq. (1a), and the DPA valley shift, given by Eq. (2), if we identified a with E_1.

We can apply Eq. (8) to a threefold T_2 state by noting that only terms in Eq. (8) with spatial dependence transforming as A_1, E, and T_2 have nonvanishing matrix elements with respect to a T_2 state. The resulting matrix elements can be conveniently written in terms of an effective Hamiltonian to be evaluated between states of pseudo-angular-momentum $L=1$. The effective Hamiltonian, including a spin-orbit term, is

$$H = \lambda \mathbf{L}\cdot\mathbf{S} + (a/2)L(L+1)(S_{11}+2S_{12})T - (G/6)\{[3L_z^2 - L(L+1)](3n_z^2-1) + 3(L_x^2-L_y^2)(n_x^2-n_y^2)\}(S_{11}-S_{12})T$$
$$-V[(L_yL_z+L_zL_y)n_yn_z + (L_zL_x+L_xL_z)n_zn_x + (L_xL_y+L_yL_x)n_xn_y]S_{44}T\ , \tag{10}$$

where

$$a = \langle x \mid U_{xx} \mid x \rangle\ ,$$
$$G = \langle x \mid U_{xx}-U_{zz} \mid x \rangle\ ,$$
$$V = \langle z \mid U_{zx} \mid x \rangle\ ,$$

and n_x,n_y,n_z are direction cosines of the applied stress with respect to cubic axes. Equation (10) is to be evaluated with respect to angular momentum basis states,

$$\Psi_1^{+1} = -(1/\sqrt{2})(x+iy)\ ,$$
$$\Psi_1^{0} = z\ , \tag{11}$$
$$\Psi_1^{-1} = (1/\sqrt{2})(x-iy)\ ,$$

and the matrix elements of $\underline{U}$ are taken with respect to basis states transforming as x, y, and z. In obtaining Eq. (10) we have used obvious relationships between matrix elements of the $\underline{U}$ components with respect to x, y, and z. If $a=E_1$, $G=E_2$, and $V=0$, Eq. (10) yields the same result as the EMA with the wave functions given by Eq. (1c) and the DPA valley shift given by Eq. (3).

The electric-dipole operator transforms as T_2 in T_d symmetry, and hence electric-dipole transitions are allowed only between the A_1 ground state and T_2 excited states. In fact, $1s(A_1)\rightarrow 1s(T_2)$ transitions should not be electric-dipole-allowed because both states have the same parity. However, parity can be mixed by interaction with neighboring defects, leading to weak absorptions. $1s(A_1)\rightarrow 1s(T_2)$ transitions have been observed for Bi in Si (binding energy $\sim$0.07 eV), and an EMA-DPA analysis based on a Hamiltonian of the form of Eq. (10) gave an excellent fit to the stress dependence of the spectrum.[12] The deformation-potential parameter G found necessary to fit the spectrum was only slightly less than the $1s\rightarrow np$ deformation potential E_2, and the measured spin-orbit parameter λ was very close to that calculated for Bi in Si.[13] We have applied Eq. (10) to the analysis of the $1s(A_1)\rightarrow 1s(T_2)$ spectrum observed for the D center (see Sec. IV A), and find that the results differ strongly from the EMA-DPA expectations.

C. Spectra of donors outside the EMA-DPA: C_{3v} or D_{3d} symmetry

Although some puzzles still remain in the analysis of the spectra, there are good indications that the A, B, and C centers have C_{3v} (or D_{3d}) symmetry, with their symmetry axes randomly distributed along $\langle 111 \rangle$ directions. We discuss the C_{3v} case; the treatment for D_{3d} symmetry is essentially the same.

In C_{3v} symmetry, T_2 states decompose into A_1+E states. To take account of the C_{3v} symmetry, we regroup combinations of the U's appearing in Eq. (8) to transform as bases of irreducible representations of this group with a symmetry axis along [111]. The result is

$$H_{\rm str} = a_1\Delta + \tfrac{1}{6}G_1\epsilon_1 + \tfrac{1}{6}G_2\epsilon_2 + V_{A_1}\tau_{A_1} + \tfrac{1}{6}V_1\tau_1 + \tfrac{1}{6}V_2\tau_2\ , \tag{12}$$

where

$$V_{A_1} \equiv \tfrac{1}{3}(U_{yz}+U_{zx}+U_{xy}),\quad A_1\ ,$$
$$\left.\begin{aligned} V_1 &\equiv 2U_{xy}-U_{yz}-U_{zx},\\ V_2 &\equiv \sqrt{3}(U_{yz}-U_{zx}),\end{aligned}\right\} E\ , \tag{12a}$$

$$\tau_{A_1} \equiv \epsilon_{yz}+\epsilon_{zx}+\epsilon_{xy},\quad A_1\ ,$$
$$\left.\begin{aligned} \tau_1 &\equiv 2\epsilon_{xy}-\epsilon_{yz}-\epsilon_{zx},\\ \tau_2 &\equiv \sqrt{3}(\epsilon_{yz}-\epsilon_{zx}),\end{aligned}\right\} E\ , \tag{12b}$$

and the remaining terms are defined in Eqs. (8a) and (8b). Equation (12) represents the strain Hamiltonian for a center with a C_{3v} symmetry axis along the [111] direction. For equivalent centers with symmetry axes along the other $\langle 111 \rangle$ directions, the energy due to an applied stress can be found by an obvious identification of the equivalent stress with respect to the particular $\langle 111 \rangle$ axis.

In C_{3v} symmetry, the $1s(T_2)$ state breaks up into A_1 and E states, and the electric-dipole operator breaks up into A_1 and E parts. On the basis of symmetry, electric-

dipole transitions should be possible between $A_1 \leftrightarrow A_1'$, $A_1 \leftrightarrow E'$, $E \leftrightarrow E'$, and $E \leftrightarrow A_1'$. As we have noted, however, the distinctions between A_1 and A_1' and between E and E' are, in general, not significant for C_{3v} symmetry, since a perturbation of C_{3v} symmetry mixes A_1 and A_1' as well as E and E'.

Applying Eq. (12) to the strain energy of an A_1' level that transforms according to Eq. (6d),

$$\mathscr{E} = \mathscr{E}_0 + a(S_{11}+2S_{12})T + \tfrac{2}{3}VS_{44}(n_y n_z + n_z n_x + n_x n_y)T \ , \tag{13}$$

where

$$a = \langle A_1' \mid a_1 \mid A_1' \rangle \ ,$$

$$V = \tfrac{3}{2}\langle A_1' \mid V_{A_1} \mid A_1' \rangle \ ,$$

and n_x, n_y, n_z are direction cosines of applied stress with respect to cubic axes, with axes chosen so that the C_{3v}-symmetry axis is along [111]. Since a perturbation of C_{3v} symmetry mixes A_1 and A_1', Eq. (13) applies to A_1 as well as A_1' states. In D_{3d} symmetry, the distinction between A_1 and A_1' remains, and the general result for A_1 is of the form given by Eq. (9) with the V term absent.

From Eq. (12), the effective Hamiltonian describing the splitting under stress of a twofold-degenerate E' level in C_{3v} symmetry can be written

$$\begin{aligned} H = {} & [a(S_{11}+2S_{12})T - (V/3)S_{44}(n_y n_z + n_z n_x + n_x n_y)T]\underline{I} \\ & + \underline{\sigma}_z[(G/6)(S_{11}-S_{12})(3n_z^2-1)T + (V'/3)S_{44}(2n_x n_y - n_y n_z - n_z n_x)T] \\ & - \underline{\sigma}_x[(G/6)(S_{11}-S_{12})\sqrt{3}(n_x^2-n_y^2)T + (V'/3)S_{44}\sqrt{3}(n_y n_z - n_z n_x)T] \ , \end{aligned} \tag{14}$$

where $\underline{I}$ is the 2×2 identity matrix, $\underline{\sigma}_z$ and $\underline{\sigma}_x$ are the Pauli matrices,

$$\underline{\sigma}_z = \begin{bmatrix} 1 & 0 \\ 0 & -1 \end{bmatrix}, \quad \underline{\sigma}_x = \begin{bmatrix} 0 & 1 \\ 1 & 0 \end{bmatrix},$$

$$a \equiv \langle E_a \mid a_1 \mid E_a \rangle, \quad V = -3\langle E_a \mid V_{A_1} \mid E_a \rangle \ ,$$

$$G \equiv \langle E_a \mid G_1 \mid E_a \rangle, \quad V' = \tfrac{1}{2}\langle E_a \mid V_1 \mid E_a \rangle \ ,$$

and E_a represents the E' basis function transforming as $2z - x - y$. Equation (14) is the Hamiltonian with respect to two basis states transforming as E_a and $E_b = \sqrt{3}(x-y)$. In obtaining Eq. (14), we have made use of the symmetry relations among matrix elements of operators transforming as bases of the C_{3v} group.[14] It should again be kept in mind that the x,y,z axes are chosen so that the C_{3v}-symmetry axis of the center is along [111]. The distinction between E and E' levels is not significant in C_{3v} symmetry, since a C_{3v} perturbation mixes E and E'. The V and V' in Eqs. (13) and (14) are defined as shown because in the simplest limit they become $\langle z \mid U_{zx} \mid x \rangle$, the quantity defined as V in Eq. (10). The distinction between E and E' states remains in D_{3d} symmetry. For E' in D_{3d}, Eq. (14) holds. For E in D_{3d}, and also for E in T_d, the energy levels are described by Eq. (14), but with the V and V' terms absent because of the parity of E states.

IV. ANALYSIS OF SPECTRA FOR S IN Si

A. *D* center (binding energy 0.6136 eV)

The D center has been identified by spin-resonance experiments[11] as an isolated S^+ ion in a site of T_d symmetry. The $1s \rightarrow np$ spectrum for this center is He^+-like,[3] confirming definitively that the center is singly ionized. Our results with uniaxial stress also confirm that the center is in a site of T_d symmetry,[3] but, as in the spin-resonance experiments, these results do not distinguish between a substitutional site and an interstitial site. Recent theoretical calculations[15] show that the substitutional site has lower energy, indicating that the D center is substitutional.

Figures 3 and 4 show, respectively, representative absorption spectra observed for the $1s \rightarrow np$ and $1s \rightarrow 1s$ transitions of the D center under applied stress. The variation of the peak energies with stress is summarized in Figs. 5 and 6. In Fig. 5 we have indicated the relative intensities expected from the DPA expression, Eq. (5), for polarizations parallel and perpendicular to the stress axis. The $1s \rightarrow np$ spectra under stress are in excellent agreement with DPA predictions for transitions from a S^+ $1s(A_1)$ ground state to effective-mass np states, in regard to both the stress dependence of the p-level energies and the selection rules [see Appendix, Eq. (A12)]. However, in the absence of stress there are two $1s \rightarrow 2p_0$ absorption lines, rather than the single line predicted by the EMA. The stress dependence and selection rules are the same for both lines.

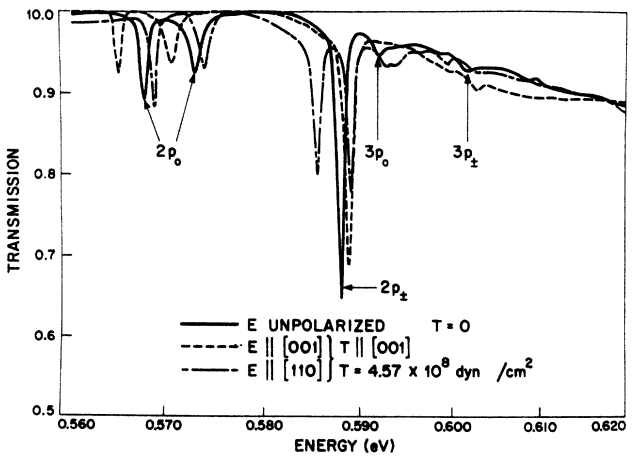

FIG. 3. Absorption spectra for the $1s(A_1) \rightarrow np$ transitions of the D center at zero stress and under uniaxial stress applied along the [001] axis.

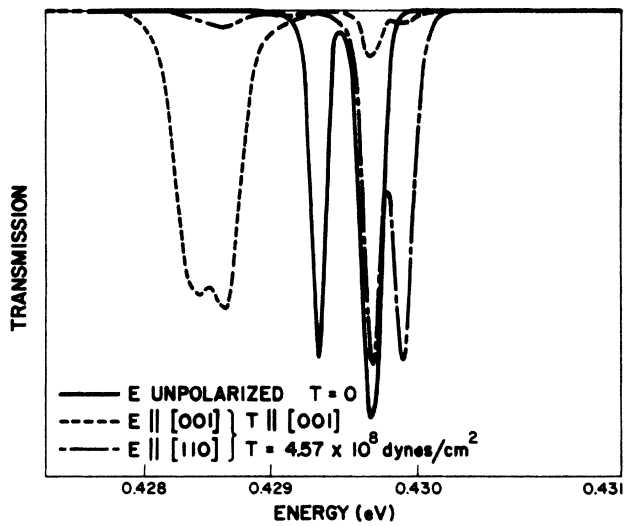

FIG. 4. Absorption spectra for the $1s(A_1)\rightarrow 1s(T_2)$ transitions of the D center at zero stress and under uniaxial stress applied along the [001] axis.

By fitting the stress dependence of the $1s\rightarrow np$ spectra, using Eqs. (3) and (9) together with published[16] values of the elastic compliance coefficients for Si ($S_{11}=0.768\times10^{-12}$ cm^2/dyn, $S_{12}=-0.214\times10^{-12}$ cm^2/dyn, and $S_{44}=1.26\times10^{-12}$ cm^2/dyn), we obtain a pure shear deformation potential $E_2=8.1$ eV and $E_1(np)-[a(A_1)]_{gr}\cong 1.7$ eV, where gr designates the ground state. (These and the other parameter values obtained for all four S centers are collected in Table III.) This value of E_2 is lower than the value of $\sim 10-11$ eV obtained from spin-resonance experiments on shallow donors in Si.[17,18] The discrepancy may be due in part to the nonideal shape of our samples, which does not closely approximate the long rodlike shape necessary to make inhomogeneous stresses negligible. Nevertheless, there appears to remain a real discrepancy for which we have no explanation.

The $1s\rightarrow 1s$ spectrum can be fitted reasonably well by assuming that transitions take place from the $1s(A_1)$ ground state to the excited $1s(T_2)$ state, which is spin-orbit-split in the absence of stress. Both the energies and relative line intensities can be fitted with a Hamiltonian for the T_2 state of the form given by Eq. (10), with parameters $a(T_2)-[a(A_1)]_{gr}\cong 1$ eV, $G(T_2)\cong 2.6$ eV, $V(T_2)\cong -0.15$ eV, and $\lambda\cong 0.22$ meV (see Fig. 6).

In the absence of the V parameter, the highest-energy transition for T along the [111] axis would not be split. The one serious discrepancy is the splitting of the lowest-frequency line for T applied along the [001] axis (see Fig. 4); no splitting should occur, since only Kramers degeneracy remains. It is possible that the observed splitting was produced by a nonuniformity in stress.

It should be noted that in the DPA the values for G and E_2 would be the same, and V would be zero. Thus

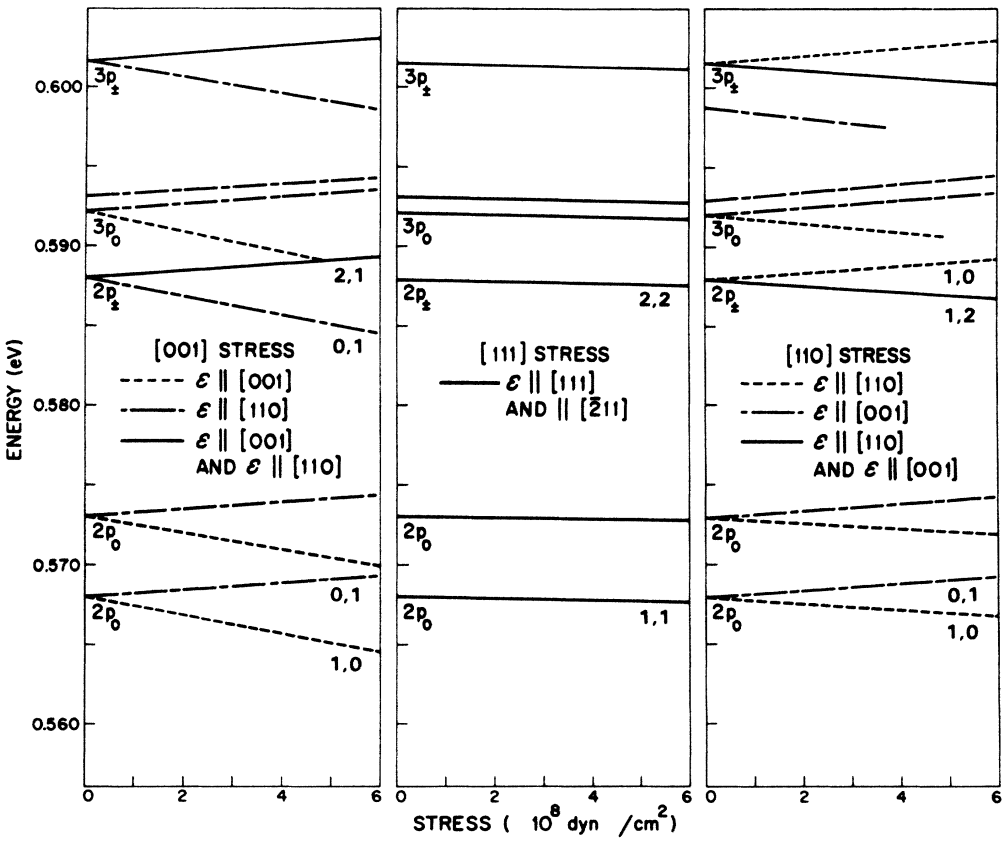

FIG. 5. Stress dependence of the peak energies for the $1s(A_1)\rightarrow np$ spectra of the D center. The pairs of numbers given for the different lines indicate relative intensities calculated at maximum stress for light polarized parallel and perpendicular to the stress axis.

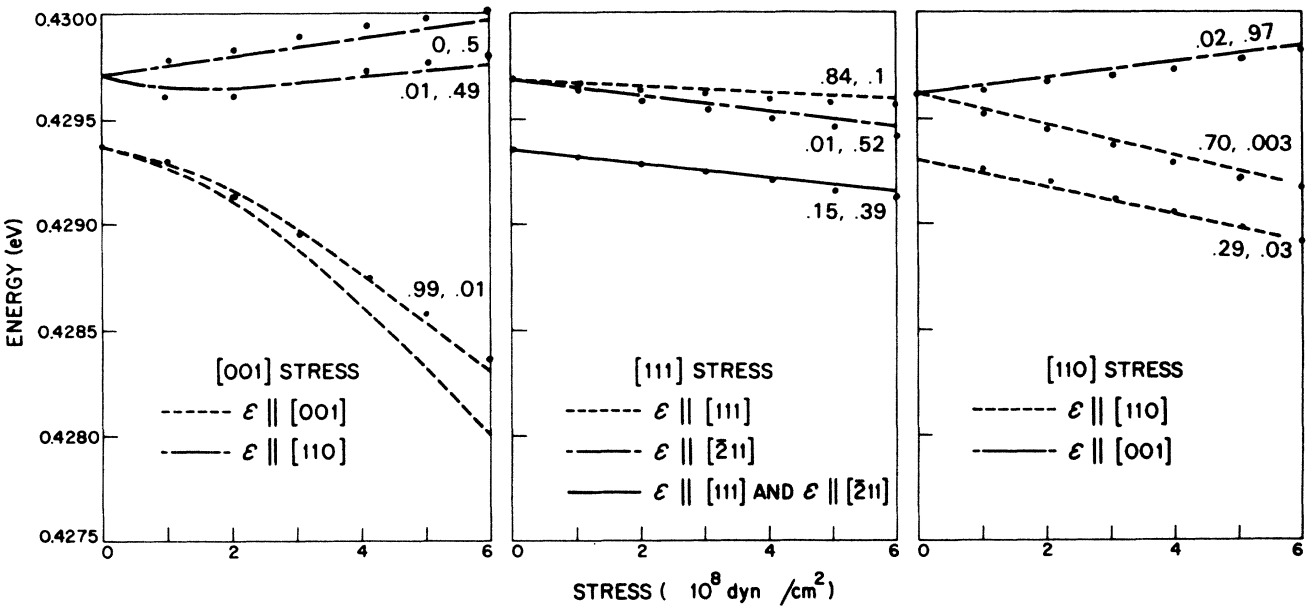

FIG. 6. Stress dependence of the peak energies for the $1s(A_1) \rightarrow 1s(T_2)$ spectra of the D center. The points are calculated for the best theoretical fit to the spectra. The pairs of numbers given for the different lines indicate relative intensities calculated at maximum stress for light polarized parallel and perpendicular to the stress axis.

the $1s(T_2)$ level of the D center, which lies only about 0.06 eV below the position of the $1s$ level in the EMA, deviates considerably from simple EMA-DPA behavior.

B. B center (binding energy 0.1877 eV)

Our B and C centers, which have respective binding energies of 0.1877 and 0.3705 eV, are shown by their $1s \rightarrow np$ spectra to be, respectively, neutral and singly ionized. We can identify these centers with centers at 0.187 and 0.368 eV that Brotherton *et al.* found from deep-level transient-spectroscopy (DLTS) data to be, respectively, neutral and singly ionized states of the same sulfur species.[19] The assignment of the B and C centers to the same sulfur species is consistent with the symmetry properties of these centers, since both appear to have C_{3v} or D_{3d} symmetry with symmetry axes distributed randomly along $\langle 111 \rangle$ directions. In addition, we can identify the C center with a center having a binding energy of 0.37 eV that Kravitz and Paul[20] have attributed to S-S pairs on the basis of their studies of spin resonance in the presence of tunable infrared radiation. We therefore conclude that the C center is probably a $(\text{S-S})^+$ pair and that the B center is a $(\text{S-S})^0$ pair, the neutral form of the same species.

Figures 7 and 8, respectively, show representative $1s \rightarrow np$ and $1s \rightarrow 1s$ spectra for the B center under an applied stress. (Our discussion will be based on C_{3v} symme-

TABLE III. Energy-level parameters for sulfur centers in silicon.

Center	Level	Energy below band edge (eV)	$a-a_{gr}$ or E_1-a_{gr} (eV)	G (eV)	V or V' (eV)	E_2 (eV)	λ (eV)
D	np		~ 1.7			8.1	
	$1s(T_2)$		~ 1	~ 2.6	~ -0.15		0.22×10^{-3}
	$[1s(A_1)]_{gr}$	0.6136					
B	np		~ 0			7.8	
	$1s(A_1')$		~ 1.5		~ 0		
	$1s(E')$		~ 1.5	10.5	~ 0		
	$[1s(A_1)]_{gr}$	0.1877			~ 2.0		
C	np		~ 0			7.8	
	$1s(E)$		~ 3.2	± 8.6	$\sim \pm 1.6$		
	$[1s(A_1)]_{gr}$	0.3705			$\sim \pm 2.0$		
A	np		~ -1.2			8.2	
	$[1s(E)]_{gr}$	0.1095		± 7.2	$\sim \pm 2.2$		

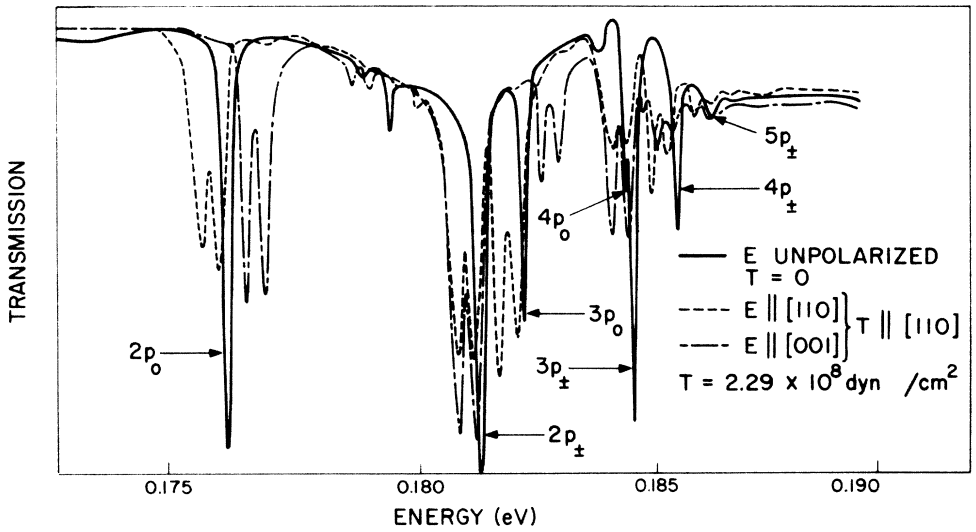

FIG. 7. Absorption spectra for the $1s(A_1)\rightarrow np$ transitions of the B center at zero stress and under uniaxial stress applied along the [110] axis.

try, although a site of D_{3d} symmetry cannot be ruled out on the basis of our spectroscopic observations.) Figures 9 and 10 show the absorption peak energies as a function of stress. The $1s\rightarrow np$ spectra are in good agreement, with regard to both p-level spacings and selection rules, with DPA predictions for transitions from the $1s(A_1)$ ground state of a center of C_{3v} symmetry to EMA np states. Both the $1s\rightarrow np$ and the $1s\rightarrow 1s$ lines are narrow, allowing a fairly complete analysis of the spectra. The parameters obtained from the analysis, using Eq. (13) for the energy of the ground state, are $E_2=7.8$ eV, $[V(A_1)]_{gr}\cong 2.0$ eV, and $E_1(np)-[a(A_1)]_{gr}\cong 0$.

The $1s\rightarrow 1s$ transitions shown in Figs. 8 and 10 can be fitted reasonably well by assigning the lines at $T=0$ at energies of 0.156 and 0.161 eV to transitions from the $1s(A_1)$ ground state to excited $1s(E')$ and $1s(A_1')$ states, respectively. This is the reverse of the identification given in the review article by Wagner *et al.*[21] Both the line energies and selection rules can be obtained by using the parameters $a(A_1')-[a(A_1)]_{gr}\cong 1.5$ eV, $V(A_1')\cong 0$, $a(E')-[a(A_1)]_{gr}\cong 1.5$ eV, $V(E')=V'(E')\cong 0$, $G(E')=10.5$ eV, and $[V(A_1)]_{gr}\cong 2.0$ eV (see Fig. 10). The one clear disagreement with theory is that the middle line for the $[1s(A_1)]_{gr}\rightarrow 1s(E')$ spectrum for T||[110] in Fig. 10 is observed to be polarized, while the theory predicts that it should be unpolarized (see Appendix).

Although the stress dependence of transition energies within the $[1s(A_1)]_{gr}\rightarrow 1s(A_1')$ and $[1s(A_1)]_{gr}\rightarrow 1s(E')$ sets is well described by the theory using Eqs. (13) and (14), the values of $a(A_1')-[a(A_1)]_{gr}$ and $a(E')-[a(A_1)]_{gr}$ required to obtain the best fit for T along difference axes are not quite the same. The discrepancy can probably be attributed to the theory's neglect of matrix elements between the excited A_1' and E' states. Such elements could arise from the spatially dependent terms of E symmetry in Eq. (12), since with increasing stress the A_1' and E' levels come close enough together to interact.

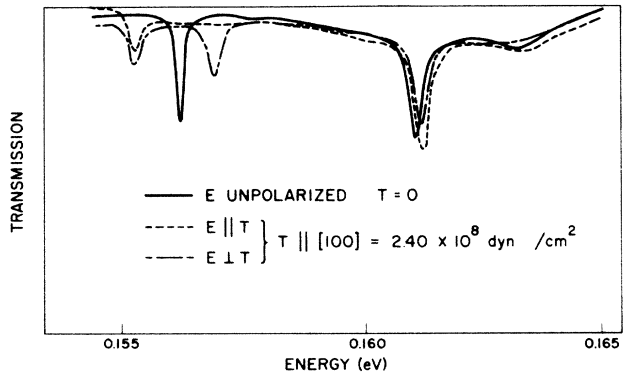

FIG. 8. Absorption spectra for the $1s(A_1)\rightarrow 1s(E')$ and $1s(A_1)\rightarrow 1s(A_1')$ transitions of the B center at zero stress and under uniaxial stress applied along the [100] axis.

C. C center (binding energy 0.3705 eV)

As mentioned in Sec. IV B, the C center is probably $(S\text{-}S)^+$. Figures 11 and 12, respectively, show representative spectra observed for $1s\rightarrow np$ and $1s\rightarrow 1s$ transitions of this center under applied stress. Figures 13 and 14 summarize the stress dependence of the absorption-peak energies.

The $1s\rightarrow np$ spectrum can be reasonably analyzed in terms of transitions from the $1s(A_1)$ ground state described by Eq. (13), although the analysis is complicated by the splittings at $T=0$ of $[1s(A_1)]_{gr}\rightarrow np_0$ transitions (see Fig. 13). In principle, the analysis of the angular dependence of the complex of lines observed as a function of stress should allow a determination of whether the splittings are produced by the basic T_d symmetry of the center, or whether they are due to the C_{3v} perturbation. In fact, the width of the lines makes the underlying structures of the spectra uncertain, and we can reach no defin-

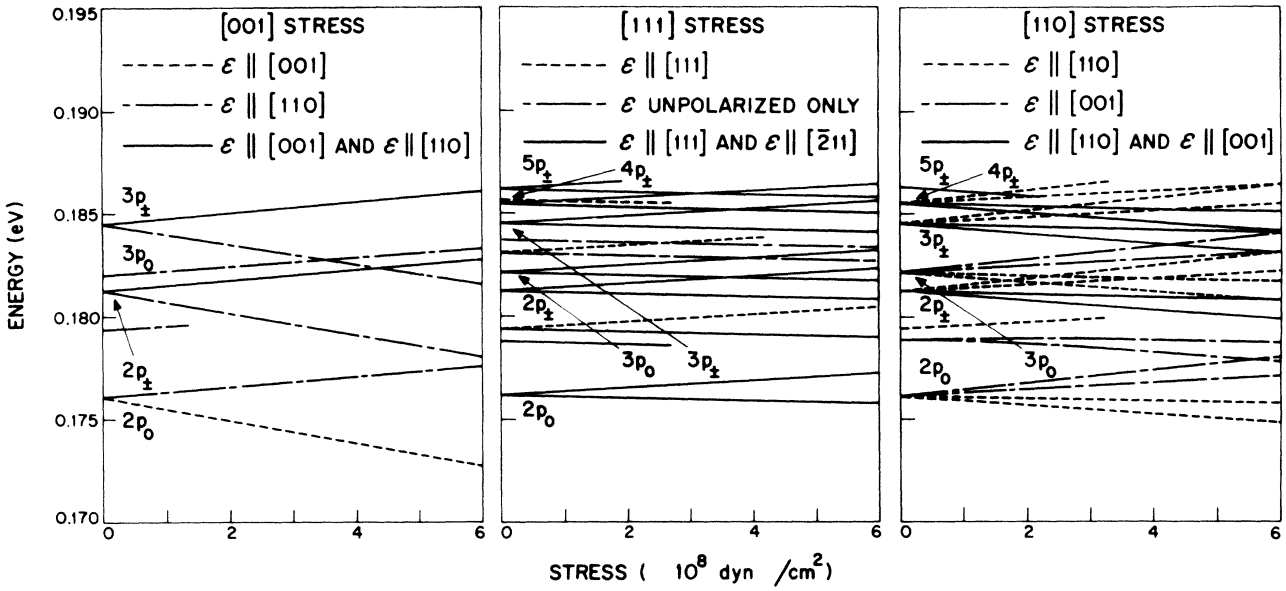

FIG. 9. Stress dependence of the peak energies for the $1s(A_1)\rightarrow np$ spectra of the B center.

ite conclusion on the origin of the $T=0$ splittings. From the general pattern of line splittings for $T\|[111]$, we estimate the magnitude of V for the ground state as $|[V(A_1)]_{gr}|\cong 2.0$ eV. The T dependence of the $[1s(A_1)]_{gr}\rightarrow 2p_\pm$ spectrum for T||[001] yields $E_2=7.8$ eV and $E_1(np)-[a(A_1)]_{gr}\cong 0$.

The $1s\rightarrow 1s$ spectrum shows considerable complexity and the lines are broad, suggesting a number of centers subject to slightly different perturbations. We can attribute the strongest features in the spectrum, at energy 0.22 eV, to transitions from a $1s(A_1)$ ground state to a $1s(E)$ excited state described by a Hamiltonian having the form of Eq. (14). This identification agrees with that given in Ref. 21. The polarization of the spectrum for T||[001] (Fig. 14) is similar to that for the $[1s(A_1)]_{gr}\rightarrow 1s(E)$ spectrum of the B center (Fig. 10), except that the polarizations of the higher- and lower-energy lines are reversed. However, the presence of a number of weaker lines makes the interpretation inconclusive. Furthermore, the perturbation due to neighboring charge centers makes the applicability of the polarization selection rules questionable. From the splittings of the strongest two lines, we obtain $|G(E)|=8.6$ eV and $a(E)-[a(A_1)]_{gr}\cong 3.2$ eV.

For T||[111], we again attribute the two strongest lines to the transition $[1s(A_1)]_{gr}\rightarrow 1s(E)$. The presence of only two strong lines can be explained if $V'\cong 0$ in Eq. (14) for

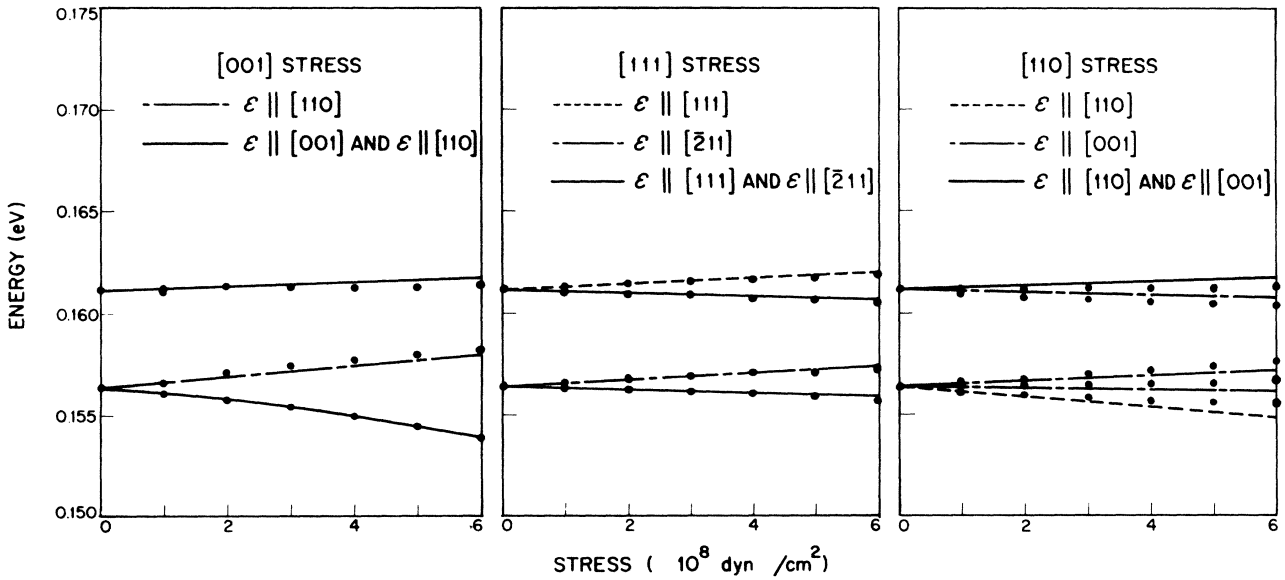

FIG. 10. Stress dependence of the peak energies for the $1s(A_1)\rightarrow 1s(E')$ and the $1s(A_1)\rightarrow 1s(A_1')$ spectra of the B center. The points are calculated for the best theoretical fit to the spectra.

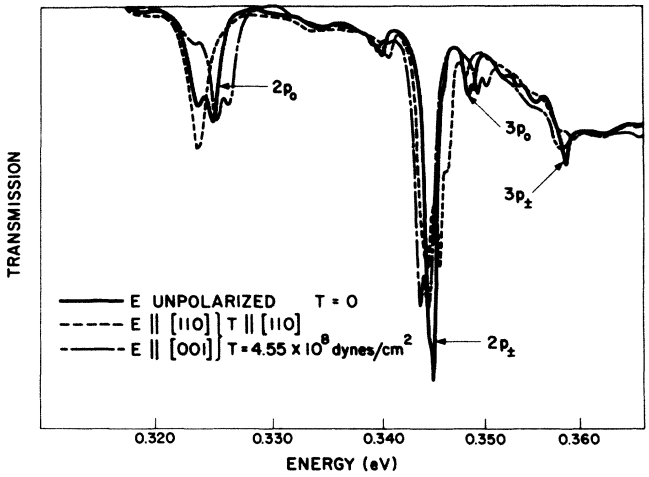

FIG. 11. Absorption spectra for the $1s(A_1)\rightarrow np$ transitions of the C center at zero stress and under uniaxial stress applied along the [110] axis.

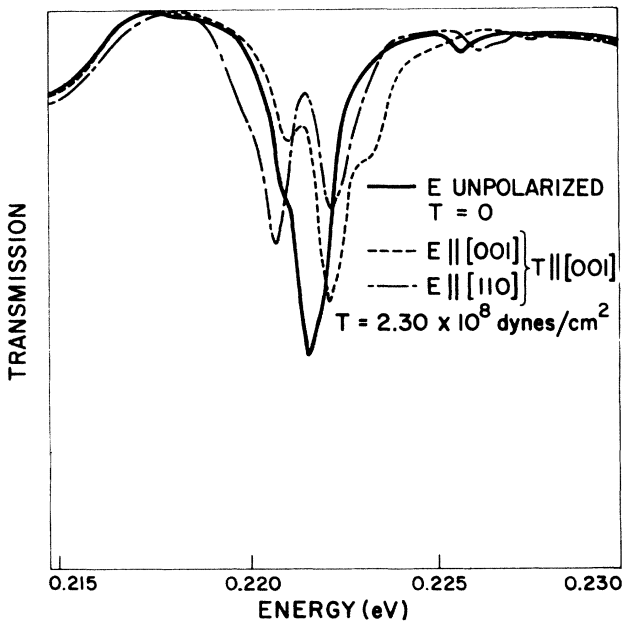

FIG. 12. Absorption spectra for the $1s(A_1)\rightarrow 1s$ transitions of the C center at zero stress and under uniaxial stress applied along the [001] axis.

the $1s(E)$ state. From the observed splitting we then find $|V(E)/2+[V(A_1)]_{gr}| \cong 1.2$ eV. Since the analysis of the $1s\rightarrow np$ spectrum led to $|[V(A_1)]_{gr}| \cong 2.0$ eV, we have either $|V(E)| \cong 1.6$ or 6.6 eV. The former value is more probable, since it seems unlikely that a level close to the effective-mass ground state would have a much larger magnitude of V than the ground state.

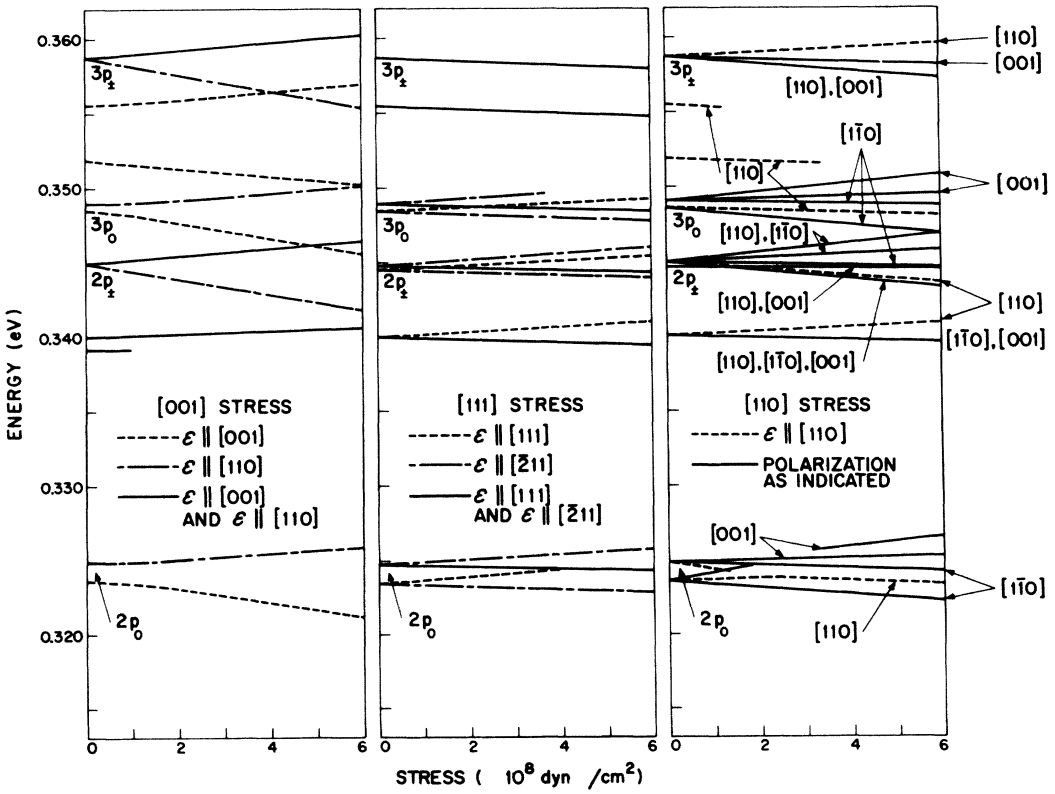

FIG. 13. Stress dependence of the peak energies for the $1s(A_1)\rightarrow np$ spectra of the C center.

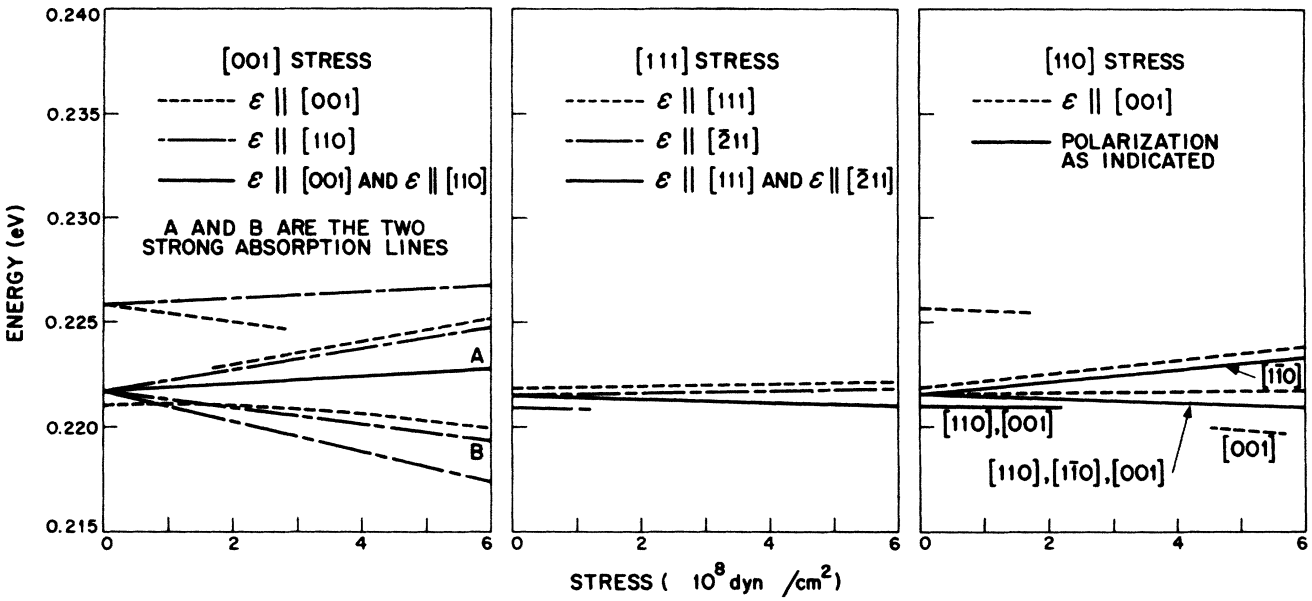

FIG. 14. Stress dependence of the peak energies for the $1s(A_1) \rightarrow 1s$ spectra of the C center. The lines marked A and B are the strongest.

D. A center (binding energy 0.1095 eV)

This center appears to be a neutral sulfur complex having C_{3v} symmetry with symmetry axes randomly distributed along ⟨111⟩ directions. The spectral lines are much narrower than those for the C center and slightly broader than those for the B center. Brotherton *et al.*,[19] using DLTS, have also observed a center in sulfur-doped Si (which they labeled the S II center) at a binding energy of 0.109 eV. The most striking property of the A center is that it seems from our analysis to have a degenerate ground state.

Figures 15 and 16, respectively, show representative $1s \rightarrow np$ and $1s \rightarrow 1s$ spectra of the A center. Figures 17 and 18 summarize the stress dependence of the absorption-peak energies. The $1s \rightarrow np$ spectra can be fitted remarkably well in frequency by assuming that the ground state is $1s(E)$ with a Hamiltonian of the form Eq. (14). The parameters obtained are $|[V(E)]_{gr}| \cong 2.2$ eV, $|[G(E)]_{gr}| = 7.2$ eV, $E_2 = 8.2$ eV, and $E_1(np) - [a(E)]_{gr}$

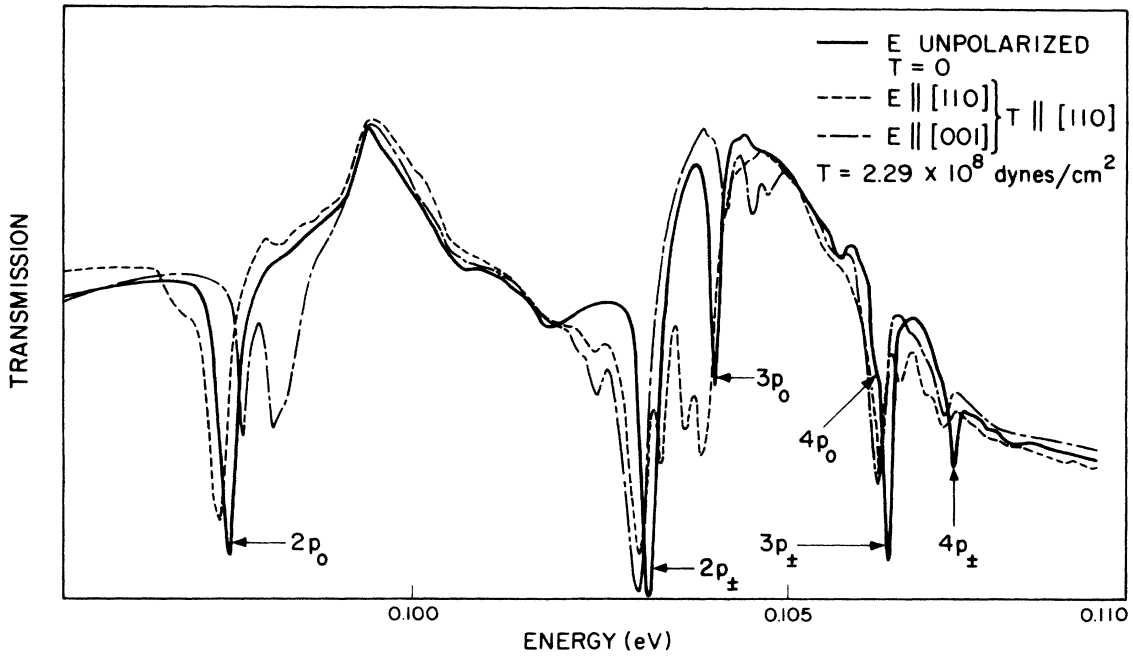

FIG. 15. Absorption spectra for the $1s \rightarrow np$ transitions of the A center at zero stress and under uniaxial stress applied along the [110] axis.

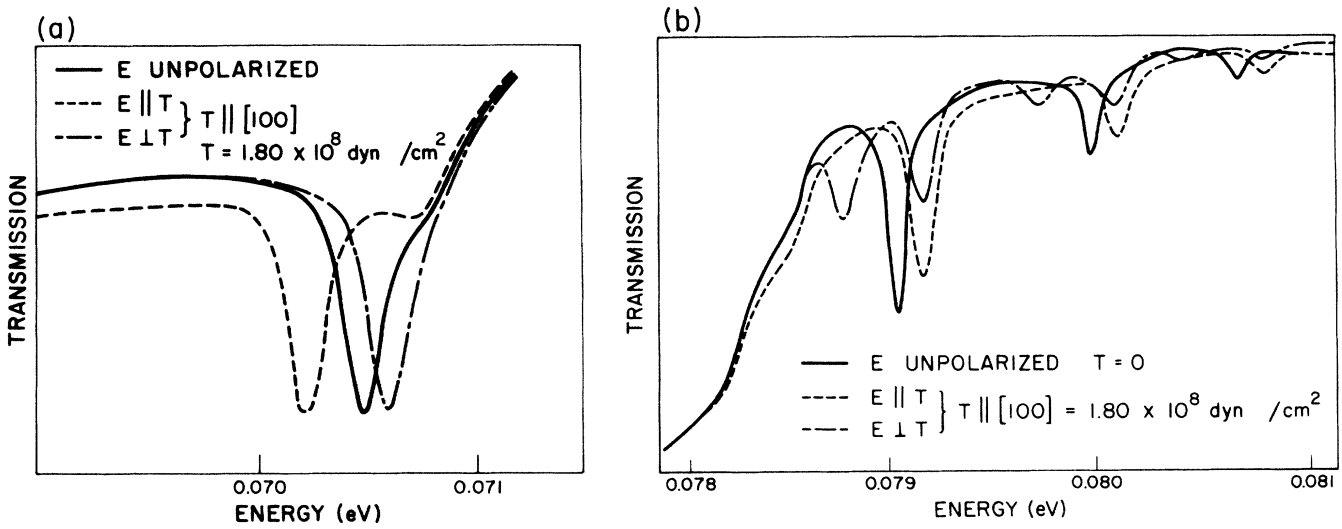

FIG. 16. Absorption spectra for the $1s \rightarrow 1s$ transitions of the A center at zero stress and under uniaxial stress applied along the [100] axis. (a) For energies in the vicinity of 0.07 eV. (b) For energies in the vicinity of 0.08 eV.

$\cong -1.2$ eV. The selection rules, however, do not entirely agree with this interpretation. In particular, for $\mathbf{T} \| [001]$ one of the four lines observed for the $1s(E) \rightarrow 2p_0$ spectrum should be "silent" rather than polarized [see Appendix, Eqs. (A16) and (A17)]. The observation of four lines can only be explained by a small misalignment or inhomogeneity of stress.

The spectra for the $1s \rightarrow 1s$ transitions of the A center remain unexplained. The three lines at an energy of ~ 0.8 eV all exhibit the same stress dependence and selection rules, for all three directions of stress. The two higher-energy lines are thus reminiscent of phonon replicas, except that the energy spacings are not constant. It has not been possible to explain the behavior of these three lines or the line at ~ 0.7 eV in terms of transitions from a $1s(E)$ ground state to either $1s(A_1)$ or $1s(E)$ excited states of C_{3v} symmetry, since the strain splittings, line multiplicities, and selection rules are inconsistent with the parameters for the $1s(E)$ ground state found by fitting the observed $1s(E) \rightarrow np$ spectra. In fact, it has not been possible to explain the $1s \rightarrow 1s$ spectra on the basis of *any* set of transitions in C_{3v} symmetry.

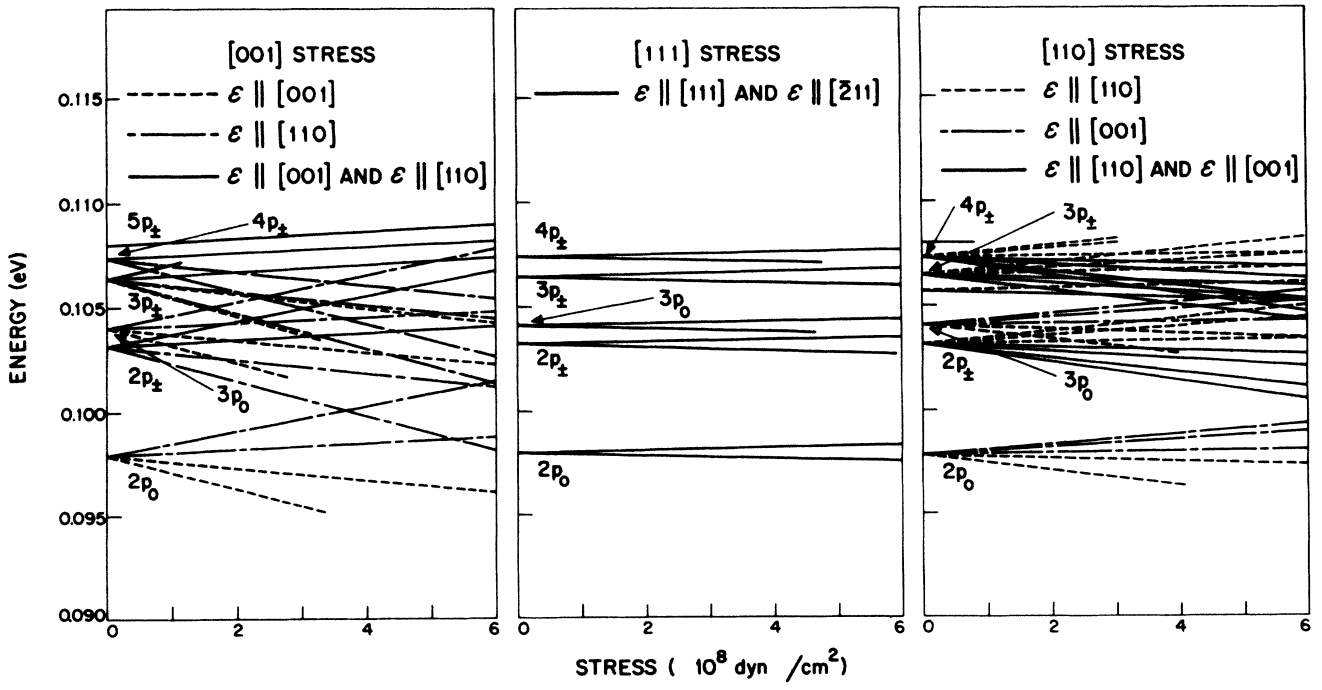

FIG. 17. Stress dependence of the peak energies for the $1s \rightarrow np$ spectra of the A center.

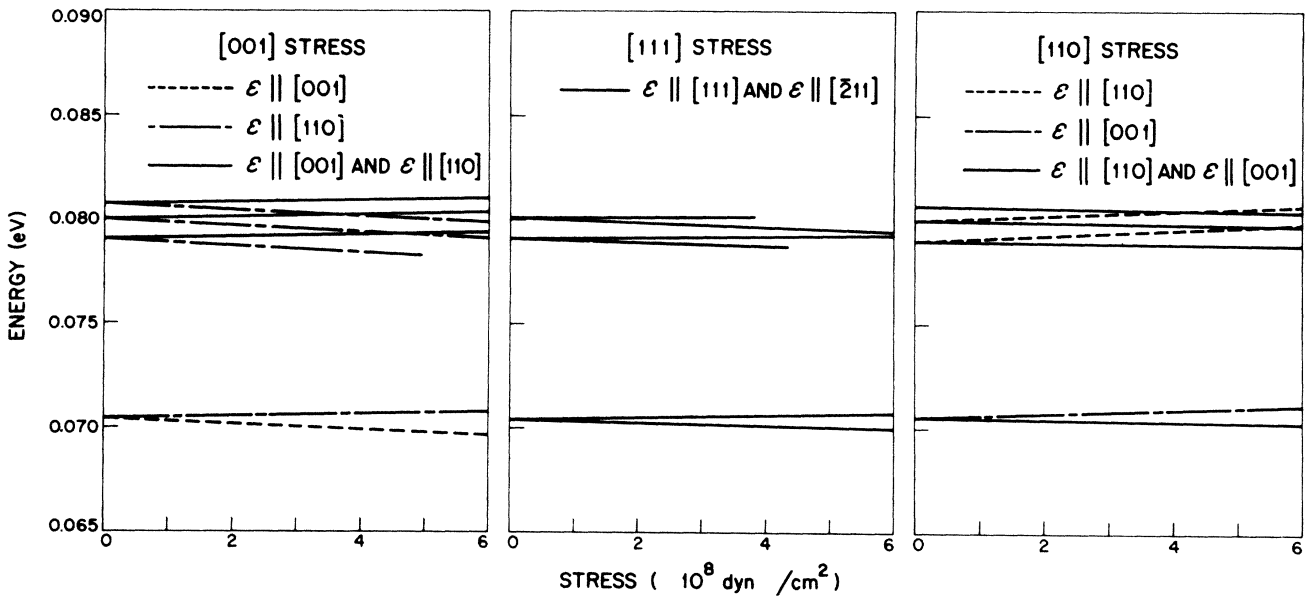

FIG. 18. Stress dependence of the peak energies for the $1s \rightarrow 1s$ spectra of the A center.

V. CONCLUSION

A number of unexplained features of the experimental results for sulfur centers in Si are worth pursuing further, both experimentally and theoretically. Although the main features of the $[1s(A_1)]_{gr} \rightarrow np$ and $[1s(A_1)]_{gr} \rightarrow 1s(T_2)$ spectra for the D center can be well explained, it is difficult to understand the occurrence of two lines for the $[1s(A_1)]_{gr} \rightarrow 2p_0$ transition. Furthermore, the observed splitting of the lowest-energy transition in the $[1s(A_1)]_{gr} \rightarrow 1s(T_2)$ spectrum of the D center for $\mathbf{T} \| [001]$ cannot be explained by the theory. It would be interesting to determine whether this splitting resulted from inhomogeneity in the stress applied to the sample.

The B center appears to be a neutral $(\text{S-S})^0$ pair. The $[1s(A_1)]_{gr} \rightarrow np$ spectra observed for this center are largely understood. The theoretical selection rules for the $[1s(A_1)]_{gr} \rightarrow 1s(A_1')$ and $[1s(A_1)]_{gr} \rightarrow 1s(E')$ transitions agree with the experimental results, except that according to the theory the middle component of the latter transition for $\mathbf{T} \| [110]$ should be unpolarized, while it is observed to be polarized. This point requires clarification.

The C center appears to be a $(\text{S-S})^+$ pair, the singly charged form of the B center. Our C-center spectra were too broad for a complete, unambiguous analysis. It would be of interest to obtain higher-resolution data in order to make a detailed study of some anomalies in the spectra, particularly the splitting of the $[1s(A_1)]_{gr} \rightarrow 2p_0$ spectrum in the absence of stress. One possibility is that this splitting is related to a central-cell perturbation for the $2p_0$ states, and is a manifestation of a breakup into A and E states in C_{3v} symmetry.

The A center is particularly interesting because of its apparently degenerate $1s(E)$ ground state. According to the Jahn-Teller theorem, a complex of C_{3v} symmetry should spontaneously distort to lift the degeneracy. However, the apparent C_{3v} symmetry of the ground state suggests that the symmetry has been restored by a dynamic Jahn-Teller effect. The $1s \rightarrow 1s$ spectra are quite puzzling, and warrant further experimental study. Until the structure of the A center is better understood, it will be difficult to construct a model of its ground state.

ACKNOWLEDGMENTS

The authors are grateful to Dr. A. J. Strauss for a careful reading of the manuscript and many helpful suggestions. This work was sponsored by the Department of the Air Force.

APPENDIX: MATRIX ELEMENTS IN THE EMA

We consider matrix elements and selection rules for electric-dipole transitions. Although our results are based on the EMA, the selection rules are related to symmetry properties and hold more generally.

We first consider matrix elements with respect to EMA $1s$-like states for Si. The wave functions can be written in the form

$$\psi_{1s}^{j} = \sum_{j} \alpha_j F_{1s}^{j}(\mathbf{r}) u_j(\mathbf{r}) e^{i\mathbf{k}_j \cdot \mathbf{r}} , \tag{A1}$$

where $F_{1s}^{j}(\mathbf{r})$ are $1s$-like envelope functions associated with the jth band edge, and $u_j(r)e^{\mathbf{k}_j \cdot \mathbf{r}}$ are Bloch functions associated with the six band edges located along cubic axes in the Brillouin zone. For convenience we define functions $\psi_{1s}^{X_1}$ (transforming as x) and $\psi_{1s}^{X_2}$ (transforming as x^2) formed by combining functions associated with x and $-x$, etc. We note that $u_{-X}(\mathbf{r}) = u_X(\mathbf{r})$ and find

$$\psi_{1s}^{X_1}=\frac{1}{\sqrt{2}}[F_{1s}^X(x^2,y^2+z^2)u_X(\mathbf{r})e^{ik_0x}-F_{1s}^X(x^2,y^2+z^2)u_X(\mathbf{r})e^{-ik_0x}]=\frac{1}{\sqrt{2}}F_{1s}^X(x^2,y^2+z^2)u_X(\mathbf{r})(e^{ik_0x}-e^{-ik_0x}) , \tag{A2}$$

$$\psi_{1s}^{X_2}=\frac{1}{\sqrt{2}}[F_{1s}^X(x^2,y^2+z^2)u_X(\mathbf{r})e^{ik_0x}+F_{1s}^X(x^2,y^2+z^2)u_X(\mathbf{r})e^{-ik_0x}]=\frac{1}{\sqrt{2}}F_{1s}^X(x^2,y^2+z^2)u_X(\mathbf{r})(e^{ik_0x}+e^{-ik_0x}) , \tag{A3}$$

where k_0 is the magnitude of the wave vector to the band-edge positions in k space and X,Y,Z label pairs of band edges. The form of the corresponding wave functions $\psi_{1s}^{Y_1},\psi_{1s}^{Y_2},\psi_{1s}^{Z_1},\psi_{1s}^{Z_2}$ can be obtained by cyclical permutations of x, y, and z, and of X, Y, and Z.

Equations (A2) and (A3) and their Y and Z counterparts can be used to write the effective-mass wave functions (1a)—(1c) in T_d symmetry, and these can be used to write matrix elements. For example, line intensities between states i and f at angular frequency ω are proportional to $|\langle i|\boldsymbol{\mu}\cdot\mathbf{E}|f\rangle|^2$, where $\boldsymbol{\mu}$ is the electric-dipole operator, and $\mathbf{E}$ is the electric field associated with a light wave. The dipole operator transforms as T_2, and the nonvanishing matrix elements of $\boldsymbol{\mu}$ between a $1s(A_1)$ ground state, Eq. (1a), and an excited $1s(T_2)$ state, Eq. (1c), can be calculated by making use of the symmetry of the wave functions. We obtain

$$\langle 1s(A_1)|\mu_x|1s(T_2)\rangle = \int\frac{1}{\sqrt{3}}(\psi_{1s}^{X_2^*}+\psi_{1s}^{Y_2^*}+\psi_{1s}^{Z_2^*})\mu_x(\psi_{1s}^{X_1})d\tau , \tag{A4}$$

with analogous expressions for the nonvanishing matrix elements of μ_y,μ_z.

Although the matrix element given by Eq. (A4) is symmetry allowed, it will be very small. We can see this by expanding Eq. (A4) and noting that all the resulting noncanceling integrals contain in their integrands products of high-spatial-frequency exponential terms and terms like $F_{1s}^{X^*}\mu_xF_{1s}^X$, etc. In the EMA, since F_{1s}^X, F_{1s}^Y, and F_{1s}^Z have negligible high-spatial-frequency components to cancel those in the exponential factors, those integrals will be negligibly small. To the extent that the EMA is violated, these integrals will contribute to the matrix elements. In the EMA, then, (A4) reduces to zero and $1s(A_1)\rightarrow 1s(T_2)$ is parity forbidden. However, the effect of perturbations such as fields due to charged neighbors can mix the parities of the $1s$-like levels and modify (A4), producing a small intensity for a $1s(A_1)\rightarrow 1s(T_2)$ transition.

On the other hand, the matrix elements of $\boldsymbol{\mu}$ between a $1s(A_1)$ level and an np level are not small in the EMA. To evaluate these matrix elements, we introduce the functions

$$\psi_{np_m}^{X_1}=\frac{1}{\sqrt{2}}F_{np_m}^Xu_X(\mathbf{r})(e^{ik_0x}-e^{-ik_0x}) , \tag{A5}$$

$$\psi_{np_m}^{X_2}=\frac{1}{\sqrt{2}}F_{np_m}^Xu_X(\mathbf{r})(e^{ik_0x}+e^{-ik_0x}) , \tag{A6}$$

where $m=0,\pm,F_{np_m}^X$ are the np-state envelope functions associated with the X-band edges, and $0,\pm$ refer to angular-momentum-component states with respect to principal axis X. The envelope functions are of the form

$$F_{np_m}^X=F_{np}^X(x^2,y^2+z^2)f_m^X , \tag{A7}$$

where

$$f_0^X=x,\quad f_\pm^X=\mp\frac{1}{\sqrt{2}}(y\pm iz) . \tag{A8}$$

The functions $\psi_{np_m}^{X_1}$ and $\psi_{np_m}^{X_2}$ consist of factors that transform, respectively, as x and x^2 with respect to the variable x, multiplied by f_m^X, which brings in additional dependence on x, y, and z. The corresponding functions for band edges along Y and Z are obtained by permuting x, y, and z. Combining the expressions (A5) and (A6) with the $1s(A_1)$ wave function, Eq. (1a), we find, for the nonvanishing matrix elements of $\boldsymbol{\mu}$ in T_d symmetry and the EMA,

$$\begin{aligned}\langle 1s(A_1)|\boldsymbol{\mu}|np_m^X\rangle &= \int\frac{1}{\sqrt{3}}(\psi_{1s}^{X_2^*}+\psi_{1s}^{Y_2^*}+\psi_{1s}^{Z_2^*})\boldsymbol{\mu}\psi_{np_m}^{X_2}d\tau\\ &=\frac{1}{\sqrt{3}}\int(F_{1s}^{X^*}\boldsymbol{\mu}F_{np}^Xf_m^X)|u_X|^2d\tau .\end{aligned} \tag{A9}$$

Since $|u_X|^2$ has the lattice periodicity and the factor in parentheses varies slowly over many lattice spacings, we can write

$$\begin{aligned}\langle 1s(A_1)|\boldsymbol{\mu}|np_m^X\rangle &\simeq\frac{1}{\sqrt{3}}\int(F_{1s}^{X^*}\boldsymbol{\mu}F_{np}^Xf_m^X)d\tau\int_{\substack{\text{unit}\\\text{cell}}}|u_X|^2d\tau\\ &\simeq\frac{1}{\sqrt{3}}\int(F_{1s}^{X^*}\boldsymbol{\mu}F_{np}^Xf_m^X)d\tau\end{aligned} \tag{A10}$$

if $u_X(\mathbf{r})$ is normalized over a unit cell. If we define $\mu_\pm\equiv\mu_y\pm i\mu_z$, $\mu_0\equiv\mu_x$, the nonvanishing matrix elements of $\boldsymbol{\mu}$ can be written

$$\begin{aligned}\langle 1s(A_1)|\mu_x|np_0^X\rangle &= \frac{1}{\sqrt{3}}\int(F_{1s}^{X^*}\mu_0F_{np_0}^X)d\tau ,\\ \langle 1s(A_1)|\mu_\mp|np_\pm^X\rangle &= \frac{1}{\sqrt{3}}\int(F_{1s}^{X^*}\mu_\mp F_{np_\mp}^X)d\tau ,\end{aligned} \tag{A11}$$

where

$$F_{np_0}^X\equiv F_{np}^Xx,\quad F_{np_\pm}^X\equiv F_{np}^X\times[(\mp)(y\pm iz)] .$$

Generalizing Eq. (A11) to any pair of band edges, we then find that the intensity of a $1s(A_1)\rightarrow np$ transition in T_d symmetry for the jth band-edge pair, which is proportional to the matrix element squared of $\boldsymbol{\mu}\cdot\mathbf{E}$, is proportional to

$$I_{np_\pm}^j=(\hat{\mathbf{E}}\times\hat{\mathbf{j}})^2|M_{np_\pm}|^2,\quad I_{np_0}^j=(\hat{\mathbf{E}}\cdot\hat{\mathbf{j}})^2|M_{np_0}|^2 , \tag{A12}$$

where

$$\begin{aligned}M_{np_\pm} &= \frac{1}{2}\times\frac{1}{\sqrt{3}}\int F_{1s}^*\mu_\mp F_{np_\pm}d\tau ,\\ M_{np_0} &= \frac{1}{\sqrt{3}}\int F_{1s}^*\mu_0F_{np_0}d\tau ,\end{aligned} \tag{A13}$$

evaluated for any band edge, and $\mu_{\mp}$ and μ_0 refer, respectively, to components of μ perpendicular and parallel to that band-edge vector. Equation (A12), which is included in the paper as Eq. (5), has been used to calculate the $1s \rightarrow np$ intensities in the EMA.

For the A center, we find that the energies of the $1s \rightarrow np$ spectrum can be fitted very well by assuming that the center has C_{3v} (or D_{3d}) symmetry and that the ground state is a $1s(E)$ state (see Sec. IV D). The intensities can be calculated by using any combination of Eqs. (6b) and (6c) for the ground state (assuming C_{3v} symmetry) and evaluating matrix elements of the μ operator. The results obtained in the EMA, by arguments similar to those used in obtaining (A10), are

$$\langle 1s(E_a) \mid \mu \mid np_m^X \rangle = -\frac{1}{\sqrt{6}} \int F_{1s}^{X*} \mu F_{np_m}^X d\tau ,$$

$$\langle 1s(E_a) \mid \mu \mid np_m^Y \rangle = -\frac{1}{\sqrt{6}} \int F_{1s}^{Y*} \mu F_{np_m}^Y d\tau , \quad \text{(A14)}$$

$$\langle 1s(E_a) \mid \mu \mid np_m^Z \rangle = \frac{2}{\sqrt{6}} \int F_{1s}^{Z*} \mu F_{np_m}^Z d\tau ,$$

$$\langle 1s(E_b) \mid \mu \mid np_m^X \rangle = \frac{\sqrt{3}}{\sqrt{2}} \int F_{1s}^{X*} \mu F_{np_m}^X d\tau ,$$

$$\langle 1s(E_b) \mid \mu \mid np_m^Y \rangle = \frac{-\sqrt{3}}{\sqrt{2}} \int F_{1s}^{Y*} \mu F_{np_m}^Y d\tau , \quad \text{(A15)}$$

$$\langle 1s(E_b) \mid \mu \mid np_m^Z \rangle = 0 ,$$

where E_a and E_b are the E functions transforming as $2z^2-x^2-y^2$ and $\sqrt{3}(x^2-y^2)$, respectively. These relations yield for the relative intensities of $1s(E) \rightarrow np$ spectral lines,

$$I_{np_{\pm}}^j = C_j(\hat{\mathbf{E}} \times \hat{\mathbf{j}})^2 \mid M_{np_{\pm}} \mid^2 , \quad \text{(A16)}$$

$$I_{np_0}^j = C_j(\hat{\mathbf{E}} \cdot \hat{\mathbf{j}}) \mid M_{np_0} \mid^2 , \quad \text{(A17)}$$

where

$$\begin{aligned} &C_X = \tfrac{1}{2}, \quad C_Y = \tfrac{1}{2}, \quad C_Z = 2 \quad \text{for } 1s(E_a) \rightarrow np , \\ &C_X = \tfrac{9}{2}, \quad C_Y = \tfrac{9}{2}, \quad C_Z = 0 \quad \text{for } 1s(E_b) \rightarrow np , \end{aligned} \quad \text{(A18)}$$

and $M_{np_{\pm}}, M_{np_0}$ are given by (A13). Equations (A16) and (A17) predict that all $1s(E_b) \rightarrow np^Z$ transitions should be "silent" for stress applied along [001] (the z direction).

---

*Deceased.

†Present address: 1725 89th Street N.E., Bellevue, WA 98004.

[1]E. Burstein, G. S. Picus, B. Henvis, and R. Wallis, J. Phys. Chem. Solids 1, 65 (1956); G. S. Picus, E. Burstein, and B. Henvis, *ibid.* 1, 75 (1956).

[2]W. Kohn, in *Solid State Physics,* edited by F. Seitz and D. Turnbull (Academic, New York, 1955), Vol. 5, p. 257.

[3]W. E. Krag, W. H. Kleiner, H. J. Zeiger, and S. Fischler, J. Phys. Soc. Jpn. Suppl. 21, 230 (1966); W. E. Krag (unpublished).

[4]See, e.g., H. G. Grimmeiss and E. Janzen, in *Proceedings of the MRS Symposium on Defects in Semiconductors II, Boston, Mass., 1982,* edited by S. Mahajan and J. W. Corbet (North-Holland, New York, 1983), p. 33.

[5]M. Stavola, K. M. Lee, J. C. Nabity, P. E. Freeland, and L. C. Kimerling, Phys. Rev. Lett. 54, 2639 (1985).

[6]H. Brooks, in *Advances in Electronics and Electron Physics,* edited by L. Marton (Academic, New York, 1955), Vol. 7, p. 85.

[7]See, e.g., V. A. Singh, U. Lindfelt, and A. Zunger, Phys. Rev. B 27, 4909 (1983); J. Bernholc, N. O. Lipari, S. T. Pantelides, and M. Scheffler, in *Proceedings of the International Conference on Defects in Semiconductors, Oisio, Japan, 1980,* edited by R. R. Hasiguti (Institute of Physics, London, 1981), p. 1.

[8]A number of conflicting notations have been used in designating sulfur centers in Si. We use our own earlier designations. In comparing our results with those of other workers, the only reliable procedure is to use binding energies as identifiers.

[9]R. A. Faulkner, Phys. Rev. 184, 713 (1969).

[10]W. H. Kleiner and W. E. Krag, Phys. Rev. Lett. 25, 1490 (1970).

[11]G. W. Ludwig, Phys. Rev. 137, A1520 (1965).

[12]W. E. Krag, W. H. Kleiner, and H. J. Zeiger, in *Proceedings of the Tenth International Conference on the Physics of Semiconductors, Cambridge, Mass.,* edited by S. P. Keller, J. C. Hensel, and F. Stern (U.S. Atomic Energy Commission, Washington, D.C., 1970), p. 271.

[13]L. M. Roth (unpublished).

[14]G. F. Koster, J. O. Dimmock, R. G. Wheeler, and H. Statz, *Properties of the Thirty-Two Point Groups* (MIT Press, Cambridge, Mass., 1963).

[15]F. Beeler, M. Scheffler, O. Jepsen, and O. Gunnarsson, Phys. Rev. Lett. 54, 2525 (1985).

[16]W. P. Mason, *Physical Acoustics and the Properties of Solids* (Van Nostrand, New York, 1958).

[17]D. K. Wilson and G. Feher, Phys. Rev. 124, 1068 (1961).

[18]E. B. Hale and T. G. Castner, Jr., Phys. Rev. B 1, 4763 (1970).

[19]S. D. Brotherton, M. J. King, and G. J. Parker, J. Appl. Phys. 52, 4649 (1981).

[20]L. Kravitz and W. Paul (unpublished).

[21]P. Wagner, C. Holm, E. Sirtl, R. Oeder, and W. Zulehner, in *Festkörperprobleme: Advances in Solid State Physics,* edited by P. Grosse (Vieweg, Braunschweig, 1984), Vol. XXIV, p. 191.